



HAL
open science

Structural determination, dielectric and photoluminescence properties of $\text{Ba}_{0.975}\text{Ln}_{0.017}(\text{Ti}_{0.95-x}\text{Zr}_x\text{Sn}_{0.05})\text{O}_3$ ($\text{Ln} = \text{Eu}, \text{Ho}; x=0.05, 0.20$)

S. Smail, Manal Benyoussef, K. Taibi, B. Manoun, N. Bensemma, A. Souici, M. El Marssi, A. Lahmar

► **To cite this version:**

S. Smail, Manal Benyoussef, K. Taibi, B. Manoun, N. Bensemma, et al.. Structural determination, dielectric and photoluminescence properties of $\text{Ba}_{0.975}\text{Ln}_{0.017}(\text{Ti}_{0.95-x}\text{Zr}_x\text{Sn}_{0.05})\text{O}_3$ ($\text{Ln} = \text{Eu}, \text{Ho}; x=0.05, 0.20$). *Physica B: Condensed Matter*, 2021, 623, 10.1016/j.physb.2021.413365 . hal-03608399

HAL Id: hal-03608399

<https://u-picardie.hal.science/hal-03608399>

Submitted on 16 Oct 2023

HAL is a multi-disciplinary open access archive for the deposit and dissemination of scientific research documents, whether they are published or not. The documents may come from teaching and research institutions in France or abroad, or from public or private research centers.

L'archive ouverte pluridisciplinaire **HAL**, est destinée au dépôt et à la diffusion de documents scientifiques de niveau recherche, publiés ou non, émanant des établissements d'enseignement et de recherche français ou étrangers, des laboratoires publics ou privés.



Distributed under a Creative Commons Attribution - NonCommercial 4.0 International License

**Structural determination, dielectric and photoluminescence properties of
 $\text{Ba}_{0.975}\text{Ln}_{0.017}(\text{Ti}_{0.95-x}\text{Zr}_x\text{Sn}_{0.05})\text{O}_3$ (Ln = Eu, Ho; x = 0.05, 0.20)**

S. Smail^a, M. Benyoussef^b, K. Taïbi^a, B. Manoun^{c,d}, N. Bensemma^{a,e}, A. Souici^f, M. El Marssi^b, A. Lahmar^{b,*}

^a*Laboratoire de Cristallographie-Thermodynamique, Faculté de Chimie, U.S.T.H.B., BP32, Al Alia, 16111, Alger, Algérie.*

^b*Laboratoire de Physique de la Matière Condensée (LPMC), Université de Picardie Jules Verne, 33 rue Saint-Leu, 80039, Amiens Cedex 1, France.*

^c*Hassan First University of Settat, FST, Rayonnement-Matière et Instrumentation, S3M, 26000, Settat, Morocco*

^d*Materials Science and Nano-engineering, Mohammed VI Polytechnic University, Lot 660 Hay Moulay Rachid, Ben Guerir, Morocco.*

^e*Centre de Recherche Nucléaire de Birine, Ain Oussera, Djelfa, Algérie.*

^f*Laboratoire de Physico-Chimie des Matériaux et Catalyse (LPCMC), Faculté des Sciences Exactes, Université de Bejaïa, Algérie.*

Abstract

Lead-free compounds with formula $\text{Ba}_{0.975}\text{Ln}_{0.017}(\text{Ti}_{0.90}\text{Zr}_{0.05}\text{Sn}_{0.05})\text{O}_3$ (BLnZ5TS) and $\text{Ba}_{0.975}\text{Ln}_{0.017}(\text{Ti}_{0.75}\text{Zr}_{0.20}\text{Sn}_{0.05})\text{O}_3$ (BLnZ20TS) [Ln=Eu, Ho] were synthesized using the solid-state reaction technique. Scanning electron micrographs of ceramics showed a decrease in the average grain size as the Ln³⁺ radii increases. The structural study allowed the identification of tetragonal and cubic symmetries at room temperature for BLnZ5TS and BLnZ20TS, respectively. Dielectric measurements were carried out as a function of temperature and frequency. The results revealed that BLnZ5TS exhibited normal ferroelectric behavior with diffuse phase transition, whereas BLnZ20TS displayed relaxor ferroelectric properties. The diffuse phase transition parameters were determined from the modified Curie–Weiss law, while the relaxor behavior in BLnZ20TS was highlighted by a good fit to the Vogel–Fülcher relationship. The photoluminescence of the prepared specimens was investigated and the results showed that these compositions bear interest for green and red emission.

Keywords: BZT-Based ceramics; Rare earth element; Structural investigations; Dielectric properties; photoluminescence.

*Corresponding author: abdel.ilah.lahmar@u-picardie.fr

1- Introduction

Finding low cost materials as solution for replacing silicon-based semiconductors is the big challenge for this 21st century. Among the materials able to meet this requirement, lead-free perovskite compounds constitute a promising candidate. Indeed, the structural variety of this family as well as the wealth of the associate properties make from these systems a preferred choice. Disastrously, the majority of perovskites used in technological applications are lead based compounds, which are harmful for human and environment [1]. As a result, the search for efficient and environmentally friendly materials has become an alternative that attracts great attention. In this context, the Ba(Zr_xTi_{1-x})O₃ (BZT) systems have stood out owing to their potential applications in many fields [2–7]

In these systems, the introduction of Zr and Sn into the Ti (B)-site of the ABO₃ perovskites structure, promotes the diffuse phase transition and the ferroelectric relaxor behavior [8-10]. On the other hand, the incorporation of rare earth elements (Ln) in BZTS was found beneficial for improving its dielectric properties [11-17]. In fact, Ln elements are generally manifested by trivalent cations, which behave like donors. Thence, a charge disproportionality may arise while replacing Ba²⁺ by Ln³⁺ on following the equation (Kröger-Vink notation):



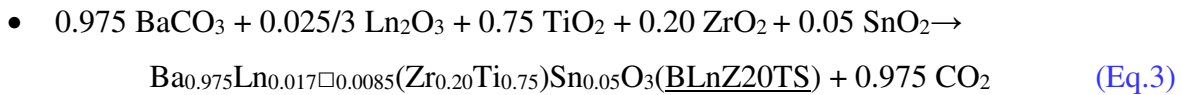
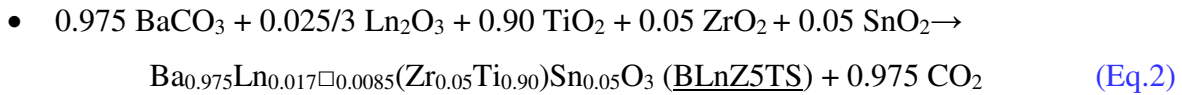
where V''_{Ba} is a cationic vacancy that required for electrical neutrality. Besides, lanthanide element is reported to inhibit the grain growth while sintering; which induce low dielectric losses [18, 19]. On the other hand, lanthanides incorporated in BZTs matrix were shown to be very effective as luminescent agents. Indeed, previous works have shown that undoped BaZr_xTi_{1-x}O₃ (BZT) exhibited a broadband photoluminescence (PL) emission spectrum, which covers the entire visible spectrum. Noting that depending on the zirconium content, the PL emission peak could be positioned in the blue-violet region between 450 and 490 nm [20]. The present work affords a contribution onto the effect of the rare-earth doped BZT system. We emphasize the synthesis and structural, ferroelectric, and photoluminescence characterizations of lead-free Ba_{0.975}Ln_{0.017 0.085}(Zr_xTi_{0.95-x})Sn_{0.05}O₃ compounds (symbolized BLnZ100xTS, Ln = Eu, Ho). This study is focused on four samples denoted BEuZ5TS, BHoZ5TS (with a low zirconium content $x = 0.05$) and BEuZ20TS, BHoZ20TS (with a higher zirconium content $x = 0.20$). These compositions are representative of the variation of Zr concentration when Ti⁴⁺ is partially replaced by Zr⁴⁺ (the Sn⁴⁺ content being kept constant) and to the substitution of Ba²⁺ by the rare earth Eu³⁺ and Ho³⁺. Our choice is justified by the fact that $x = 0.20$ corresponds to the Zr-limit concentration between classical ferroelectric

region (<0.20) and relaxor zone (> 0.20) of $\text{Ba}(\text{Ti}_{1-x}\text{Zr}_x)\text{O}_3$ (BZT) system [21]. Moreover, to limit the number of variables, we made an appropriate choice by fixing the Ln^{3+} (Eu^{3+} , Ho^{3+}) and Sn^{4+} contents respectively to 0.017 and 0.05.

2. Materials and methods

2.1 Solid state synthesis

Solid-state reaction method was used to synthesize ceramics of BLnZ100xTS ($x= 0.05$ and 0.20). The starting materials used for this study were powders of BaCO_3 , Ln_2O_3 ($\text{Ln} = \text{Eu}$, Ho), TiO_2 , ZrO_2 , and SnO_2 (all from Sigma-Aldrich, USA) of high purity ($>99.99\%$). Materials with BLnZ5TS and BLnZ20TS compositions were obtained according to the following chemical reactions:



where “ \square ” corresponds to the vacancies created during the reaction at high temperature. The starting compounds were previously dried at 200°C for 3h to eliminate any residual water in the powders. Thereafter, the powders were weighed in the stoichiometric amount to obtain the chosen composition. The obtained samples were then mixed in an agate mortar and carefully grounded for 2 h. Then, the mixture was heat-treated under air atmosphere at 1180°C for 14 h with a heating rate of $5^\circ\text{C}/\text{min}$. The obtained powder was pressed under 500 MPa into a pellet of 13 mm in diameter and about 1 mm in thickness. Finally, the obtained ceramics were heat treated at 1400°C for 4 hours under air atmosphere. Loss of weight was determined before and after heat treatment and was found to be less than 1%. Diameter shrinkages $\Delta\Phi/\Phi$ were determined as $(\Phi_{\text{initial}} - \Phi_{\text{final}})/\Phi_{\text{initial}}$. Their values were about 10% while the relative density (experimental density/theoretical density) was about 0.9.

2.2. Characterizations

The crystal structures of the sintered pellets were done using a D8 Advance X-ray diffractometer (Vantack detector) equipped with copper $\text{K}\alpha$ radiation ($\lambda=1.5405 \text{ \AA}$). The phase identification was done using the reference cards of the JCPDS Powder Diffraction File. The analysis of the obtained diffractograms was done through Rietveld refinement method based on the Fullprof program [22] integrated into the WinPLOTR software [23]. A

pseudo-Voigt profile function was found to describe adequately the obtained reflections on taking as starting positions those of BaTiO₃ compound [24].

The scanning electron microscopy analysis using a Philips SEM device (model XL30) has allowed the observation of the microstructures of the sintered samples.

The dielectric measurements were carried out on pellets using a SOLARTRON SI-1260 impedance meter. Prior, the sintered ceramics (pellet) were assimilated to capacitors by the deposition of silver paste on both faces. A LINKAM TS600 furnace was used for the thermal investigations. The thermal evolution of the permittivity and the losses were achieved in temperature (100-473 K) and frequency (10²-10⁶ Hz) range. The sample was placed in a measuring cell between two electrically insulated cylindrical electrodes. Beforehand, the samples undergo degassing under vacuum to eliminate all traces of humidity in the cell. Photoluminescence measurements were performed using a Shimadzu brand RF-6000 spectrofluorimeter. The excitation wavelengths values used are 390 and 395 nm for the Europium-based compounds and 455 nm for the Holmium-based compounds.

3. Results and discussion

3.1. Microstructural study

To examine the rare-earth doping effect on the microstructural evolution of BZTS, a scanning electron microscopy (SEM) study was performed on the investigated ceramics without going through the polishing step. Fig.1 shows the SEM micrographs of both BLnZ5TS and BLnZ20TS ceramics. As we can see from this figure, the grains appear in spherical shapes with a relatively small size. Moreover, compared to undoped BZTS, grain growth appears to be inhibited by the addition of very small amounts of rare earths [25-27]. Therefore, the average particle size of undoped BZTS (> 10 μm) is much larger than that observed for the samples BLnZ5TS and BLnZ20TS (0.2–3.6 μm). This result agrees well with some reported compound containing lanthanide element [28].

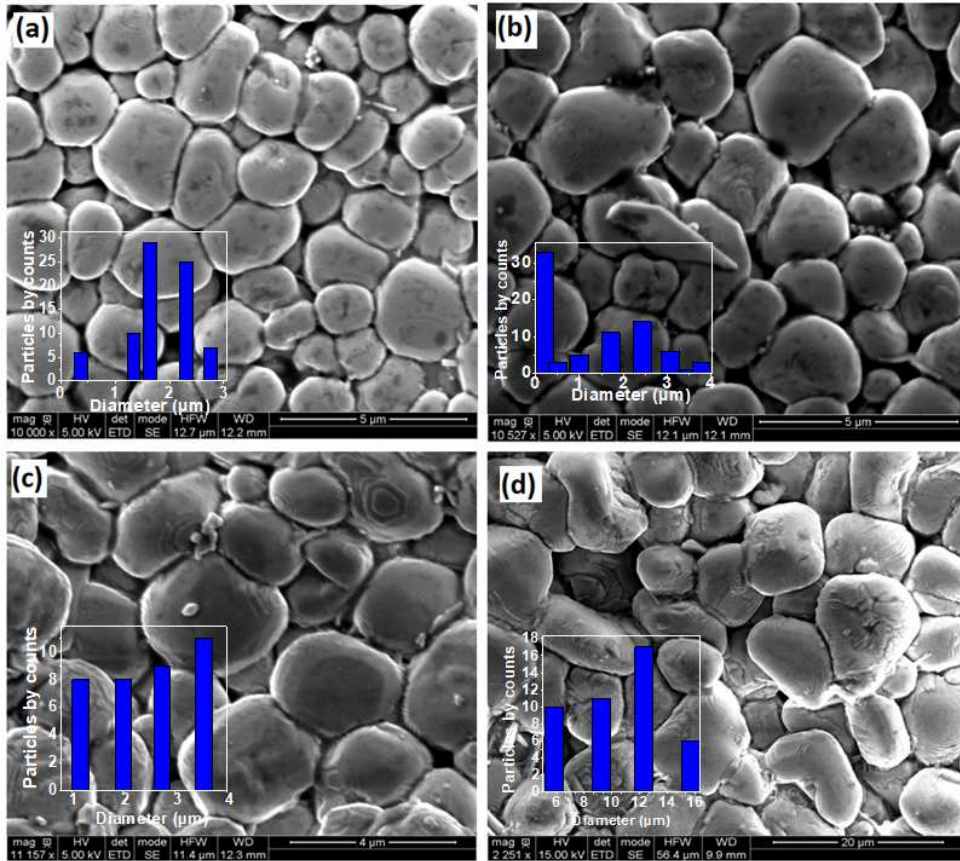


Fig. 1: SEM images for *BEuZ5TS* (a), *BHoZ5TS* (b), *BEuZ20TS* (c) and *BHoZ20TS* (d). The insets show the histogram of grain size distribution for each sample.

3.2. Room-temperature X-ray diffraction

The purity phase of *BLnZ5TS* and *BLnZ20TS* ceramics were confirmed by the X-ray diffraction at room temperature. It should be noted that the XRD profiles of the *BLnZ5TS* and *BLnZ20TS* ceramics reveal the peaks related to the perovskites phase. Nevertheless, a very weak peak, in the 2θ angle range $28-29^\circ$, was observed. This peak was identified to belong to the starting compound Ln_2O_3 . The structural Rietveld refinement was achieved assuming a tetragonal symmetry ($P4mm$ for *BLnZ5TS*) and a cubic symmetry ($Pm\bar{3}m$ for *BLnZ20TS*) [10]. The observed, calculated and the difference of the XRD patterns for all the *BLnZ5TS* and *BLnZ20TS* compositions are represented in Fig.2. The obtained results indicate the good agreement between observed XRD patterns and fitted theoretical data. However, it is concluded that *BLnZ5TS* and *BLnZ20TS* compositions crystallized at room temperature in tetragonal and cubic symmetries respectively.

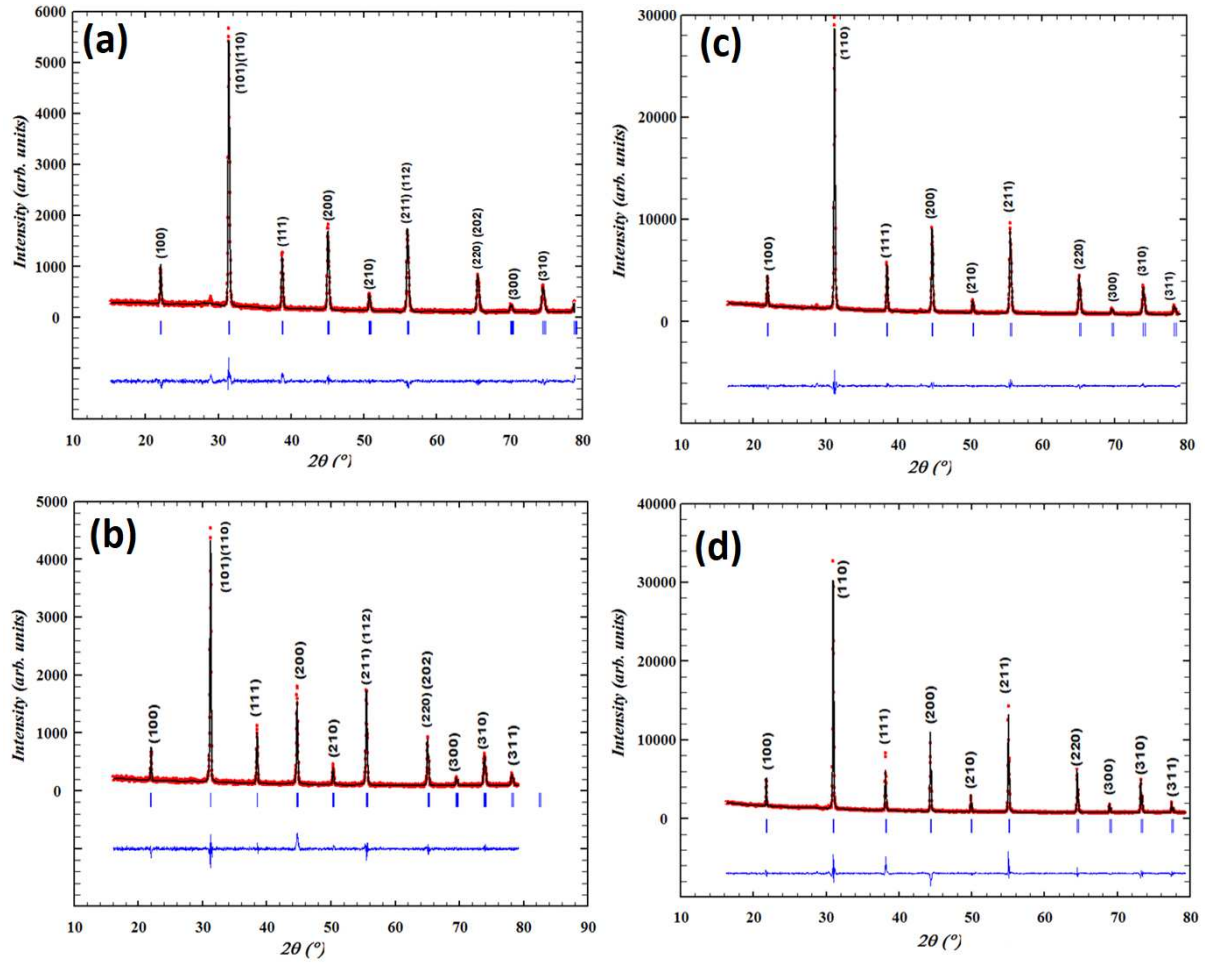


Fig. 2: Rietveld refinement plots of X-ray diffraction patterns for *BEuZ5TS* (a), *BHoZ5TS* (b), *BEuZ20TS* (c), and *BHoZ20TS* (d) (Red open circles indicate the observed data, and black solid lines indicate the calculated pattern with Rietveld method. The lower curve is the difference between observed and calculated patterns. Vertical markers spot the calculated positions of Bragg reflections).

Table 1 gathers the symmetry, lattice parameters and reliability factors acquired by Rietveld refinement. Noting that the obtained results are reported and compared to those of BaTiO_3 Tetragonal (*T*) and Cubic (*C*) as references, respectively. It appears that the compositions with higher Zr content (BLnZ20TS) have larger lattice parameters (a) and volume (V). Knowing that Sn^{4+} (0.05) and Ln^{3+} (0.017) contents are constants for BLnZ5TS and BLnZ20TS, these variations could be related to the bigger size of Zr^{4+} compared to that of Ti^{4+} ($r_{\text{Ti}^{4+}} = 0.605 \text{ \AA}$ and $r_{\text{Zr}^{4+}} = 0.720 \text{ \AA}$ in 6 Coordination Number [29]). In addition, the values of the *c/a* ratio observed in tetragonal symmetry are very close to unity, which is compatible with a pseudo-cubic symmetry for the BLnZ5TS compositions. The results of the dielectric permittivity variation presented in §.3.3 confirm our choice. Besides, in the relaxor phase, the average structure of these compounds remains cubic down to low temperature.

Table 1: Symmetry, lattice parameters and refinement reliability factors of BLnZ5TS (A) and

BLnZ20TS (B) [Ln = Eu, Ho]

(A)	BEuZ5TS	BHoZ5TS	BaTiO ₃ (T)
a=b (Å)	4.0300(4)	4.0089(6)	3.9945
c (Å)	4.0221(5)	4.0173(4)	4.0335
c/a	0.998	1.002	1.098
V(Å ³)	65.32	64.56	64.36
Space group	P4mm	P4mm	P4mm
R _B	5.88	3.66	-
R _F	3.18	2.83	-
Rwp	15.3	15.2	-
χ ²	1.95	2.08	-
(B)	BEuZ20TS	BHoZ20TS	BaTiO ₃ (C)
a=b=c(Å)	4.0616(7)	4.0586 (6)	4.0119
V(Å ³)	67.003	66.85	64.57
Space group	Pm $\bar{3}$ m	Pm $\bar{3}$ m	Pm $\bar{3}$ m
R _B	3.92	7.15	-
R _F	3.04	4.35	-
Rwp	9.18	16.3	-
χ ²	3.39	5.35	-

Table 2: Rietveld refinement results

Composition	Ions	site	X	y	Z	B _{iso}	Occupancy
BEuZ5TS	Ba ²⁺ /Eu ³⁺	1a	0	0	0.0054(2)	0.931(2)	0.975 / 0.017
	Ti ⁴⁺ /Zr ⁴⁺ /Sn ⁴⁺	1b	0.5	0.5	0.5191(3)	0.764(1)	0.90/0.05/0.05
	O ₁ ²⁻	1b	0.5	0.5	0.0265 (2)	0.123 (3)	1
	O ₂ ²⁻	2c	0.5	0	0.5599 (1)	0.900 (2)	2
BHoZ5TS	Ba ²⁺ /Ho ³⁺	1a	0	0	0.0091(3)	0.689(3)	0.975 / 0.017
	Ti ⁴⁺ /Zr ⁴⁺ /Sn ⁴⁺	1b	0.5	0.5	0.5302(3)	0.633(1)	0.90/0.05/0.05
	O ₁ ²⁻	1b	0.5	0.5	0.0248(4)	0.866(5)	1
	O ₂ ²⁻	2c	0.5	0	0.5207(5)	0.306(4)	2
BEuZ20TS	Ba ²⁺ /Eu ³⁺	1a	0	0	0	1.621(2)	0.975 / 0.017
	Ti ⁴⁺ /Zr ⁴⁺ /Sn ⁴⁺	1b	0.5	0.5	0.5	1.771(3)	0.75/0.20/ 0.05
	O ²⁻	3c	0.5	0.5	0	1.363(2)	3
BHoZ20TS	Ba ²⁺ /Ho ³⁺	1a	0	0	0	1.075(3)	0.975 / 0.017
	Ti ⁴⁺ /Zr ⁴⁺ /Sn ⁴⁺	1b	0.5	0.5	0.5	1.784(4)	0.75/0.20/ 0.05
	O ²⁻	3c	0.5	0.5	0	2.717(5)	3

Tables 2 assembles the refined atomic positions, occupancy and isotropic atomic shift parameters of BLnZ5TS and BLnZ20TS. As it can be seen, Ba²⁺ and Ln³⁺ are located in the same A-site with a fractional percentage. In addition, Ti⁴⁺/Zr⁴⁺/Sn⁴⁺ cations located in the B-sites are connected with the oxygen atoms to form (Ti⁴⁺/Zr⁴⁺/Sn⁴⁺)O₆ octahedra (see Fig. 3). Albeit, a slight variation is observed in the atomic coordination for BLnZ5TS compositions, corresponding to a shift in the direction of *c* polar axis. Furthermore, relatively good reliability factors (comparing to the standard values) are obtained and are in the range of the disordered perovskites [31, 32]. We believe that the observation of cubic symmetry at low and high temperature for the relaxor ferroelectric materials is linked to the presence of such disorder.

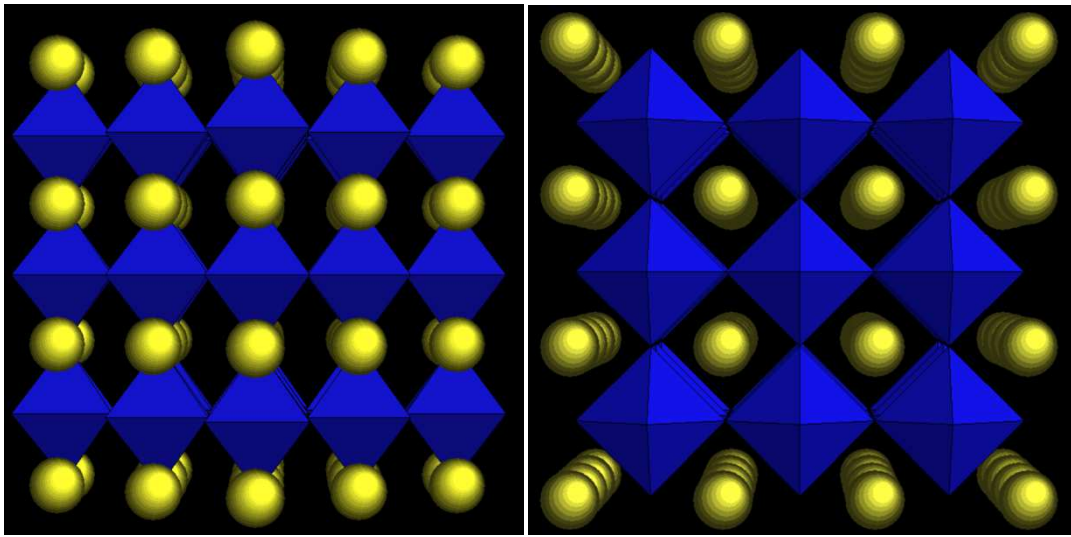


Fig. 3: View of the crystalline structure of the tetragonal *BEuZ5TS* (left) and cubic *BHoZ20TS* (right).

3.3. Dielectric study

Figs. 4(a) and (b) exhibit the temperature and frequency dependence of the permittivity (ϵ') and dielectric losses ($\tan \delta$) for BLnZ5TS samples (Ln= Eu (a), Ho (b)). At first glance, a single frequency independent peak appears which would correspond to the cubic-tetragonal phase transition similar to that observed at T_c in the well-known material BaTiO₃ (BT). However, careful observation seems to reveal the presence of the two other transitions “tetragonal-orthorhombic“ and “orthorhombic-rhombohedral” appearing respectively at temperatures noted T_1 and T_2 in the normal ferroelectric material BT. However, unlike BT where the three transitions appear clearly, in BLnZ5TS the transitions at T_1 and T_2 are manifested by a slight bump in the dielectric permittivity evolution. This bump is more or less difficult to detect depending on the nature of the doping element. Besides, the sharp peak

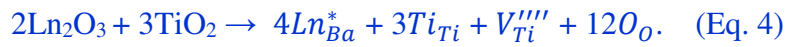
observed usually at T_C in pure BT, moved into a relatively broad peak involving a diffuse phase transition in the case of BLnZ5TS compounds. It is noteworthy that other authors have reported a similar result, affirming that the incorporation of lanthanide elements in the BZT compositions with low Zr content, led to a diffuse phase transition [33-37]. This coalescence of the three phase transitions leading to a single broad peak has been attributed to the lattice distortion and compositional fluctuation developed in the rare earth doped BZT ceramics [38, 39]. Despite the existence of a diffuse phase transition, as the temperature of the maximum permittivity (T_m) is frequency independent, the dielectric behavior of BLnZ5TS remains typical of normal ferroelectric materials. The comparison with BT shows that T_1 and T_2 are moved to higher temperatures, while T_C is shifted to lower temperatures. For example, in the case of BHoZ5TS, the second derivative of the dielectric curves (see inset of figure 3 (b)) reveals that $T_1=220$ (>183) K, $T_2=312$ (>268) K and $T_C=352$ (<393) K (recall that the three phase transitions in BT occurs respectively at $T_1=183$ K, $T_2=268$ K and $T_C=393$ K [22]). However, the values of T_1 (220 K) and T_2 (312 K) obtained by dielectric measurements would indicate an orthorhombic phase at room temperature. In order to verify this hypothesis, an attempt to refine the structure of the composition BHoZ5TS with an orthorhombic model has been done in different space groups (A_{mm2} , C_{2221} , P_{mm2} , and A_{2mm}). We did not have an improvement in the refinement in comparison with the tetragonal one. In all case there was be either a divergence or poor refinement with high reliability factors. As an example, below is the refinement results performed in the A_{mm2} space group. The obtained reliability factors are $R_{wp}=31.8$, $R_B=23.00$, $R_F=15.4$, $\chi=3.28$. In addition, the temperatures of the maximum permittivity (T_m) of BEuZ5TS and BHoZ5TS are of the same order of magnitude and appear to increase as the size of the lanthanide decreases.

Otherwise, when the Zirconium concentration increases ($x = 0.20$), a second type of dielectric behavior is highlighted. Figs. 4 (c) and (d) show the thermal and frequency variation of the permittivity ($\epsilon'r$) and dielectric losses ($\tan \delta$) for BLnZ20TS compositions according to the nature of the rare earth element (Ln = Eu (c), Ho (d)). The thermal and frequency changes in the permittivity revealed a single broad peak characteristic of a diffuse phase transition, with an up shift of the related position. In this case, the ferroelectric behavior is of the relaxor nature. The maximum permittivity temperatures (T_m) vary from 167 K to 189 K and seem to increase when the rare earth size decreases.

In addition, it should be noted that low dielectric losses have been emphasized for both BLnZ5TS and BLnZ20TS compositions. As we can see in Table 3, the dielectric losses show low values whether for BLnZ5TS ($0.015 < \text{tg}\delta < 0.023$) or for BLnZ20TS ($0.023 < \text{tg} \delta <$

0.030). This range of low dielectric losses is suitable for practical applications. Besides, our results are consistent with literature data asserting that doping ferroelectric perovskites with rare earth elements leads to a drop in the dielectric losses [40, 41].

According to the Eq.1, every two Ln^{3+} substituting ions one A-site vacancy is created for charge neutrality, which produces compositional fluctuation on a microscopic scale. Bhargavi et al. [38] reported that such a vacancies change the order- disorder and local symmetry that influence widely the physical properties. On the other hand, Chou et al. [18] reported that the substitution of Ba by Lanthanide is accompanied by the creation of Ti-vacancy according the equation:



The simultaneous existence of Ln_{Ba}^* and V_{Ti}'''' might lead to a compensation defect that can explain the low dielectric loss observed in Ln-doped BZT systems. An other possibility, the presence of secondary phase can also favorite oxygen defects that compensate Ba-sites vacancies. All these mechanisms are reported to decrease the dielectric loss and improved the dielectric properties of BZT systems.

B LnZ5TS and B LnZ20TS compositions are also illustrious by the $\text{Ba}^{2+}/\text{Ln}^{3+}$ substitution. Table 3 displays clearly that, for a fixed value of the Zr content, T_C (or T_m) increases when the rare-earth radii decreases ($r_{(\text{Eu}^{3+})} = 1.2945 \text{ \AA} > r_{(\text{Ho}^{3+})} = 1.234 \text{ \AA}$ in 12 Coordination Number). For instance, T_m (B EuZ5TS) = 331K and T_m (B HoZ5TS) = 352 K; T_m (B EuZ20TS) = 167 K and T_m (B HoZ20TS) = 189 K. This evolution seems to be in contradiction with the previous results reported about the cation (A^{n+}) located outside the octahedron in ABO_3 perovskites [42].

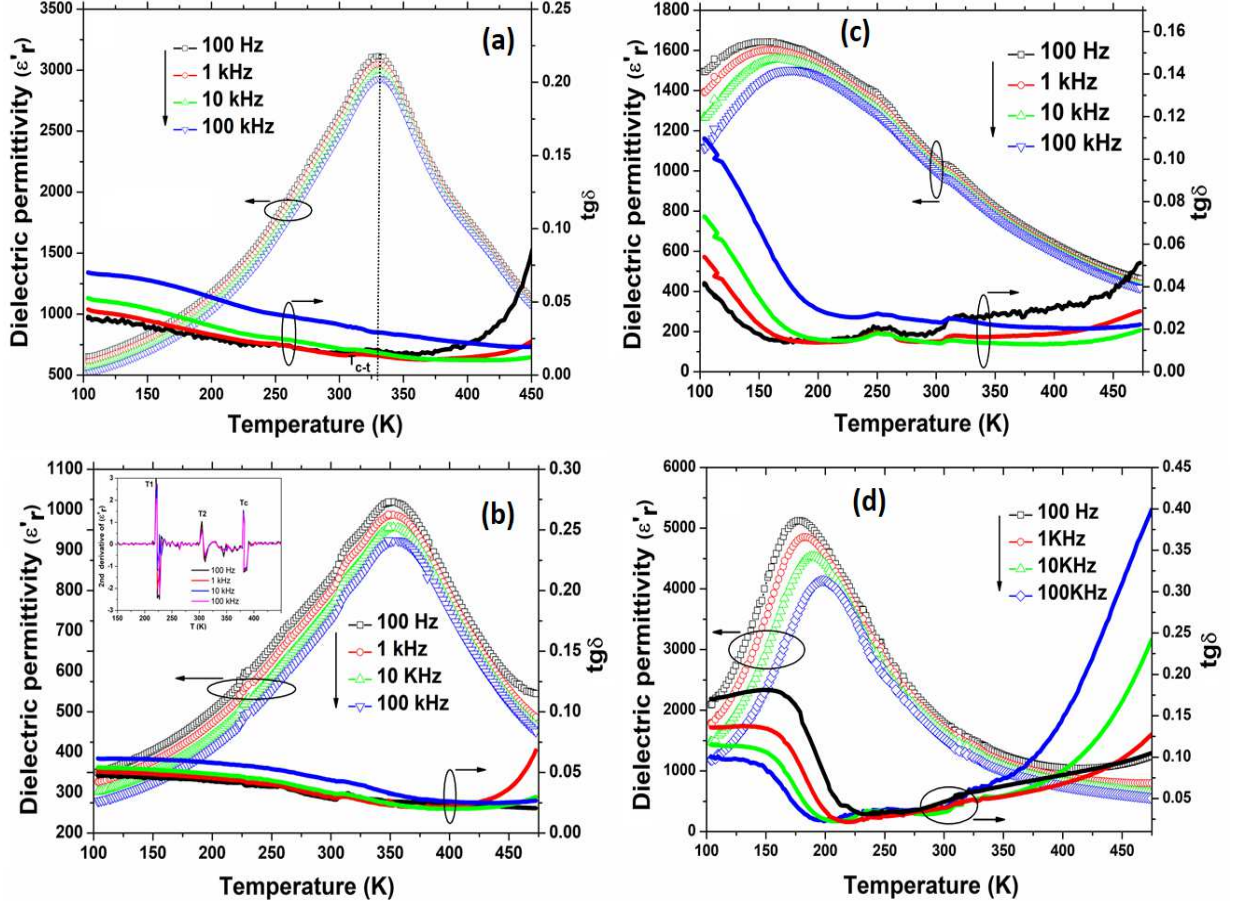


Fig. 4: Temperature dependence of the dielectric permittivity and dielectric loss for *BEuZ5TS* (a), *BHoZ5TS* (b), *BEuZ20TS* (c), and *BHoZ20TS* (d).

Table 3: Dielectric characteristics of *BLnZ5TS* and *BLnZ20TS* compositions at 10 kHz

Compounds	BLnZ5TS		BLnZ20TS	
	Eu	Ho	Eu	Ho
T_1 (K)	-	220	-	-
T_2 (K)	-	312	-	-
T_C/T_m (K)	331	352	167	189
T_0 (K)	345	359	190	210
T_{dev} (K)	420	443	335	320
ΔT_m (K)	75	84	145	131
ΔT_{mf} (K)	1.5	4	16	20
$\Delta \epsilon'_T / \epsilon'_r$	0.06	0.093	0.085	0.193
γ	1.39	1.58	1.98	1.63
$C \times 10^{-5}$	1.08	0.78	0.95	1.45
ϵ'_{rmax}	2995	956	1557	4534
ϵ'_{RT}	2560	798	1039	1730
$tg \delta_{RT}$	0.015	0.023	0.023	0.030

Ravez et al. reported that the decrease of T_C is linked to the decrease in the A^{n+} ion size, as it observed for SrTiO₃-BaTiO₃ solid solution (T_C (BaTiO₃) = 400 K; T_C (Ba_{0.5}Sr_{0.5}TiO₃) = 245 K; $r_{(Sr^{2+})} < r_{(Ba^{2+})}$). Nevertheless, according to the chemical bond's theories, the decrease in the size of the ions at A or B site, leads to an increase in T_C [43]. Therefore, in our case, the decrease of T_C could be attributed to the increase of vacancies number due to the incorporation of Ln³⁺ into Ba²⁺ site [39]. Further, the greater distortion produced on the lattice structure when the ionic radii of Ln³⁺ increase led to lower values of T_C (or T_m), which is in agreement with our experimental study. From the results reported in Table 3, we notice that ϵ'_{max} (BEuZ5TS) \sim 1/3 ϵ'_{max} (BHoZ5TS) while ϵ'_{max} (BEuZ20TS) \sim 3 ϵ'_{max} (BHoZ20TS). This is probably related to an intrinsic behavior of each material (conventional ferroelectric or relaxor ferroelectric...) and to the non-homogeneous densification within these 4 compositions.

3.3.1. Diffuse phase transition parameters

The ferroelectric diffuse phase transition is characterized by a wide temperature range around T_m where the dielectric permittivity adopts its maximum value (ϵ'_{max}). Initially, the origin of the diffuse phase transition was related to the chemical heterogeneity on the microscopic scale due to the compositional fluctuations on the B-site of the ABB'O₃ complex perovskites [44]. The Curie Weiss law (Eq. 5) generally describes the diffuse phase transition:

$$\frac{1}{\epsilon'_r} = \frac{T - T_0}{C} (T > T_0) \quad (Eq. 5)$$

where C and T_0 are the Curie-Weiss temperature and Curie Weiss constant, respectively.

Fig. 5 shows the plot of $1/\epsilon'_r$ as a function of the temperature at 10 kHz and the adjustment of the experimental data by Eq. (5) according to the Curie-Weiss law. Noting that T_0 is extracted from the plot in the paraelectric region by extrapolating the reciprocal dielectric constant. The values ($T_0 > T_m$) observed for all compositions indicated the deviation from the Curie-Weiss law. Otherwise, a slight deviation from the Curie-Weiss law is observed for the compositions with a low Zr content (BEuZ5TS (Fig.5a) and BHoZ5TS (Fig.5b)) while a greater shift appears for the compositions with a higher Zr content (BEuZ20TS (Fig.5c) and BHoZ20TS (Fig.5d)). For all the studied compositions, the fitting parameters (C and T_0) are displayed in Table 3.

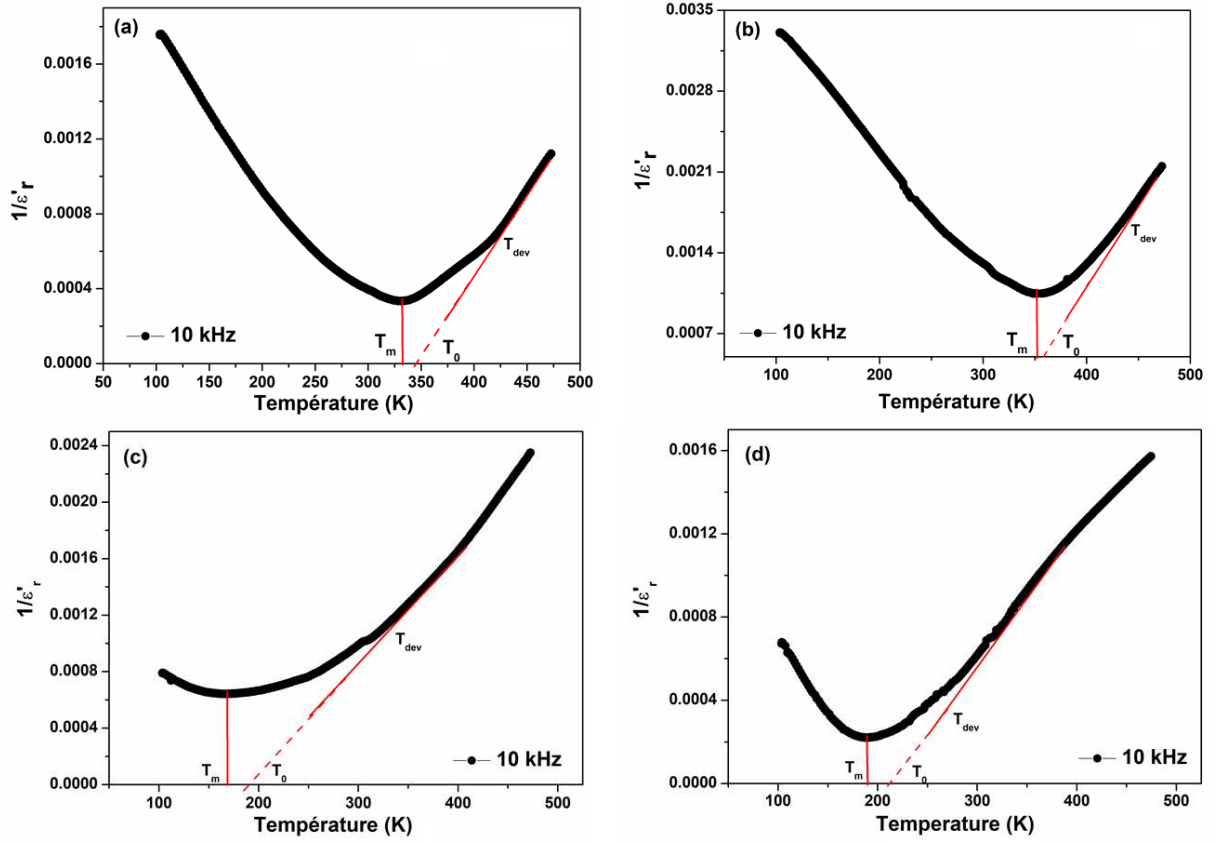


Fig 5: Thermal evolution of the inverse of the permittivity for *BEuZ5TS* (a), *BHoZ5TS* (b), *BEuZ20TS* (c), and *BHoZ20TS* (d).

To evaluate the deviation degree from the Curie-Weiss law, we have used the parameter $\Delta T_m = T_{dev} - T_m$ [41]. Where T_m represents the temperature of the permittivity maximum, whereas T_{dev} is the deviation temperature from the Curie-Weiss law. From the above relation, it emerges that when T_m is decreasing, ΔT_m increases. On the other hand, the ΔT_m values are higher in BLnZ20TS compositions indicating a more important diffusion degree compared to those of BLnZ5TS series. Knowing that T_m decreases as the Zr content increases and the Ln concentration is constant, ΔT_m should be greater for compounds with higher Zr content (BLnZ20TS). Indeed, this is what we observed in our experimental results (Table 3).

Otherwise, to describe the diffuseness in a phase transition, we used the modified Curie-Weiss law (Eq.6) [45]:

$$\frac{1}{\varepsilon_r} - \frac{1}{\varepsilon_m} = \frac{(T - T_m)^\gamma}{C} \quad (\text{Eq. 6})$$

Where ε_m corresponds to value of ε'_r and γ represents the diffuseness exponent. The C is a constant. Noting that when $\gamma = 1$, the material is a classical normal ferroelectric, in contrast a

typical relaxor ferroelectric corresponds to $\gamma = 2$. As shown in Figs.6 (a) and (b)), the plots of $\ln (1/\varepsilon'_r - 1/\varepsilon'_m)$ vs. $\ln (T - T_m)$ at 10 kHz for BLnZ5TS and BLnZ20TS compositions exhibit nearly linear variation. For all the compositions, values of $\gamma > 1$ were observed (Table 3). This involves that these compositions are characterized by a diffuse phase transition. Moreover, we noticed that the higher values of γ were obtained for zirconium-rich compositions (BLnZ20TS). On the other hand, for the two series BLnZ5TS and BLnZ20TS, we observed an irregular variation of ΔT_m and γ . However, their global values ($75 \leq \Delta T_m \leq 84$; $1.39 \leq \gamma \leq 1.58$ for BLnZ5TS) and ($131 \leq \Delta T_m \leq 145$; $1.63 \leq \gamma \leq 1.98$ for BLnZ20TS) confirmed that the diffusion degree parameters (ΔT_m , γ) are greater for the BLnZ20TS compositions (i.e. compositions with high Zr content)

3.3.2. Relaxor characteristics

In addition to the diffuse phase transition, the relaxor behavior is marked by the frequency dependence of T_m and ε'_r . This distinctive behavior can be evaluated from the parameters noted ΔT_{mf} and $\Delta\varepsilon'_r/\varepsilon'_r$ as indicated respectively on the (Eq. 7) and (Eq. 8) below.

$$\Delta T_{mf} = T_m(10^6 \text{ Hz}) - T_m(10^2 \text{ Hz}) \quad (\text{Eq. 7}) \quad \frac{\Delta\varepsilon'_r}{\varepsilon'_r} = \frac{\varepsilon'_r(10^2 \text{ Hz}) - \varepsilon'_r(10^6 \text{ Hz})}{\varepsilon'_r(10^2 \text{ Hz})} \quad (\text{Eq. 8})$$

The frequency dispersion is more significant as ΔT_{mf} and $\Delta\varepsilon'_r/\varepsilon'_r$ values are higher. In Table 3 are summarized the obtained parameters determined according to the following inequalities:

$$\begin{array}{ll} \text{BLnZ5TS:} & 1.5 \leq \Delta T_{mf} \leq 4 & 0.060 \leq \Delta\varepsilon'_r/\varepsilon'_r \leq 0.093 \\ \text{BLnZ20TS:} & 16 \leq \Delta T_{mf} \leq 20 & 0.085 \leq \Delta\varepsilon'_r/\varepsilon'_r \leq 0.193 \end{array}$$

From these inequalities, the very low values of ΔT_{mf} (≤ 4) and $\Delta\varepsilon'_r/\varepsilon'_r$ (≤ 0.093) corroborate the very low frequency dispersion for BLnZ5TS as we reported previously (§3.3.1). Therefore, despite the presence of the diffuse phase transition, BLnZ5TS does not present a relaxor behavior. On the contrary, the high values of ΔT_{mf} (> 16) and $\Delta\varepsilon'_r/\varepsilon'_r$ (> 0.085) denote an important diffusion degree and frequency dispersion in BLnZ20TS ceramics. Consequently, it turns out that these compositions behave like relaxor ferroelectric materials. Some of these compositions show T_m close to 300 K. This is the case of the conventional ferroelectric of BLnZ5TS compositions. For BLnZ20TS compositions exhibiting a relaxor ferroelectric behavior, they are distinguished by low values of T_m and relatively high values of ε'_{rmax} .

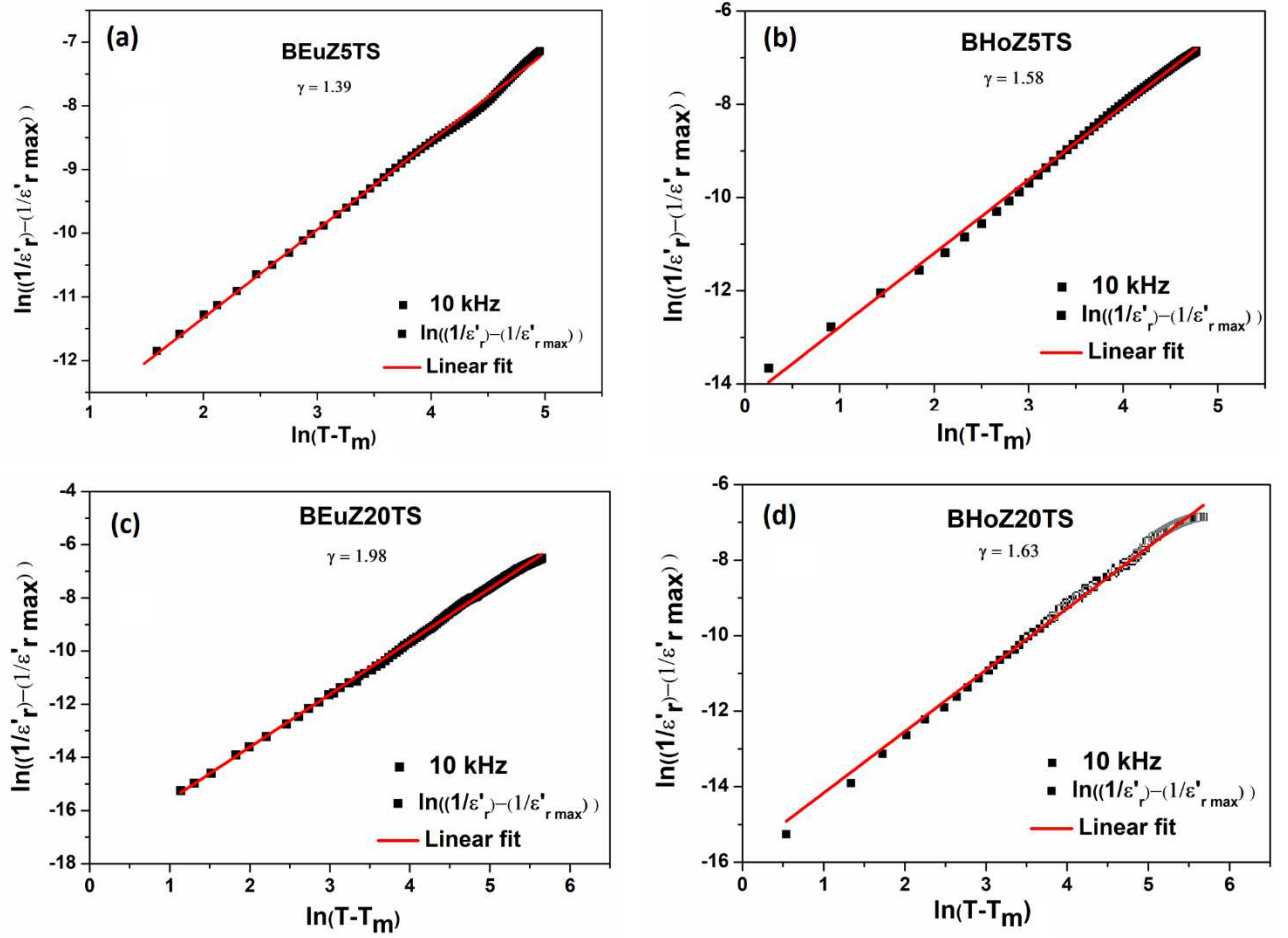


Fig.6: Variation of $\log (1/\epsilon'_r - 1/\epsilon'_{r \max})$ as a function of $\log (T - T_m)$ at 10 kHz for the ceramics $BLnZ5TS$ and $BLnZ20TS$ [$Ln=Eu, Ho$]

3.3.3. Vogel-Fulcher approach

The empirical Vogel-Fülcher (V-F) equation can also give sound information about relaxor ferroelectric behavior. It can be expressed as (Eq. 9) [46].

$$f = f_0 \exp \frac{-E_a}{k_b(T_m - T_g)} \quad (\text{Eq. 9})$$

where f_0 is the attempt frequency, E_a represents a measure of average activation energy, k_B and T_g are the Boltzmann's constant and freezing temperature, respectively

Figs.7 show the plot of $\log (f)$ vs T_m for the BEuZ20TS and BHoZ20TS relaxor samples. The experimental curve was fitted using the above V-F formula. The fitting parameters of the V-F relation were reported in **Table 4**. The close agreement of the data with the V-F relationship suggests a relaxor like behavior for the two compositions. On the other hand, it can be noted that as $r_{(Ln3+)}$ increases, the fitting parameters of V-F (E_a and f_0) decrease. Basing on the report of L.E. Cross, the obtained result is a signature of a higher

barrier existence between two wells, along with an enlargement in the potential well [47]. It should be mentioned that the BLnZ20TS compositions have some similitudes with $\text{Ba}(\text{Ti}_{1-x}\text{Zr}_x)\text{O}_3$ relaxor compositions ($x > 0.20$). Indeed, a large peak of dielectric permittivity depending on the frequency and the temperature characterizes these ferroelectric relaxors. This effect is generally attributed to the presence of nanometric polar regions. To determine the nature of these regions, a study of the local structure was carried out within the relaxor compositions $\text{Ba}(\text{Ti}_{1-x}\text{Zr}_x)\text{O}_3$ [48]. It revealed the existence of deformed ZrO_6 octahedra able to generate a local polarization, responsible for the frequency dispersion observed experimentally. On the other hand, among the samples studied through this work, $\text{Ba}_{0.975}\text{Eu}_{0.017}\text{Zr}_{0.05}\text{Sn}_{0.05}\text{Ti}_{0.90}\text{O}_3$ and $\text{Ba}_{0.975}\text{Ho}_{0.017}\text{Zr}_{0.20}\text{Sn}_{0.05}\text{Ti}_{0.75}\text{O}_3$ based ceramics showed interesting dielectric characteristics. Table 5, reports the values of some dielectric properties of BEuZ5TS and BHoZ20TS extracted respectively from Figs. 6. Data corresponding to similar compositions, taken from the reported literature are also included. This table is shared into two sections corresponding respectively to the comparisons of Zr-poor compositions ($x = 0.05$ and 0.10) and those of relatively Zr-rich compositions ($x = 0.20$). We notice the good performance of $\text{Ba}_{0.980}\text{Ho}_{0.020}\text{Zr}_{0.10}\text{Ti}_{0.90}\text{O}_3$ [37]. Apart from this composition, it emerges from this table that the dielectric characteristics are clearly improved for BEuZ5TS and BHoZ20TS compositions. However, it should be noted herein that the relatively weak value of $T_m = 189$ K (far from room temperature) was obtained for the compound BHoZ20TS.

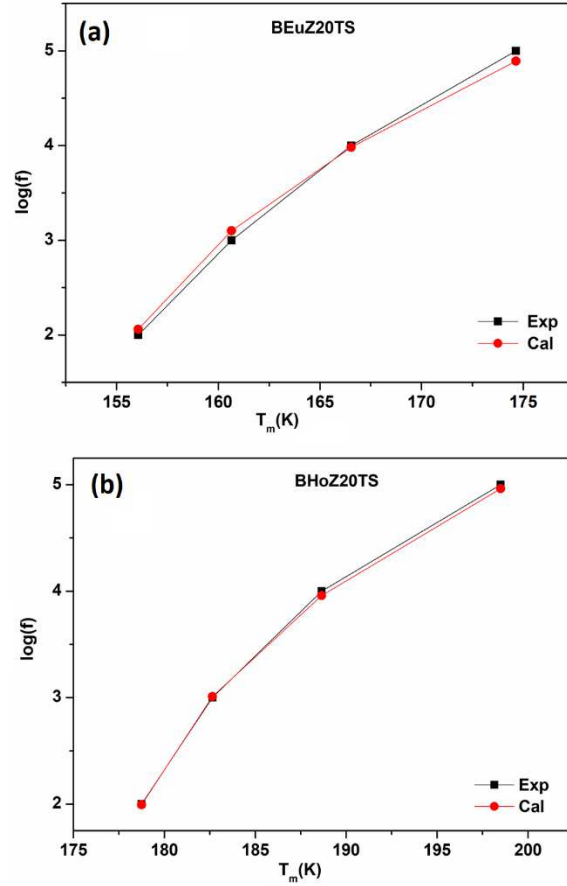


Fig.7. Plots of $\log(f)$ as a function of T_m for the compositions BEuZ20TS and BHoZ20TS

Table 4. Vogel-Fülcher Parameters of BLnZ20TS compositions

Compositions	Tg (K)	Ea (eV)	Ln f_0
BEuZ20TS	144	0.012	14.73
BHoZ20TS	158	0.024	18.52

Table 5: Some dielectric characteristics for Ln-doped BZT derived ceramics at 10 kHz.

Compositions	T_m	$\epsilon'_{r(max)}$	$\epsilon'_{(RT)}$	$\text{tg}\delta_{(RT)}$	γ
Ba _{0.975} Eu _{0.017} Zr _{0.05} Sn _{0.05} Ti _{0.90} O ₃ [This work]	331	2995	2560	0.015	1.39
Ba _{0.980} Eu _{0.013} Zr _{0.05} Ti _{0.95} O ₃ [38]	378	2400	1600	0.05	1.63
Ba _{0.980} Gd _{0.013} Zr _{0.05} Ti _{0.95} O ₃ [39]	400	2400	1800	0.03	1.37
Ba _{0.980} Ho _{0.02} Zr _{0.10} Ti _{0.90} O ₃ [37]	270	9979	8644	0.01	1.97
Ba _{0.975} Ho _{0.017} Zr _{0.20} Sn _{0.05} Ti _{0.75} O ₃ [This work]	189	4534	1730	0.03	1.63
Ba _{0.980} La _{0.020} Zr _{0.20} Ti _{0.80} O ₃ [26]	242	2661	2000	0.05	1.84
Ba _{0.980} La _{0.020} Zr _{0.20} Ti _{0.80} O ₃ [27]	250	2242	1700	0.10	1.89

3.3.4. Approach of phase transition by Raman spectroscopy

To approach the phase transition in the studied system, we give in figure 8 the thermal variation of Raman spectra of B₁EuZ₁T₁S sample as an example. The assignment of the Raman modes is carried out by analogy with the BZT phase [17]. The spectrum consists of six distinguished modes 110, 186, 256, 301, 518 and 720 cm⁻¹ corresponding respectively to the following modes: E(TO₁), A₁(TO₁), A₁(TO₂), B/E(TO+LO), A₁(TO₃) and A₁(LO₃). The detailed room temperature Raman study about the influence of rare earth amount on the structural transition can be found in our previous work dealt with Lanthanum (La³⁺) element [17].

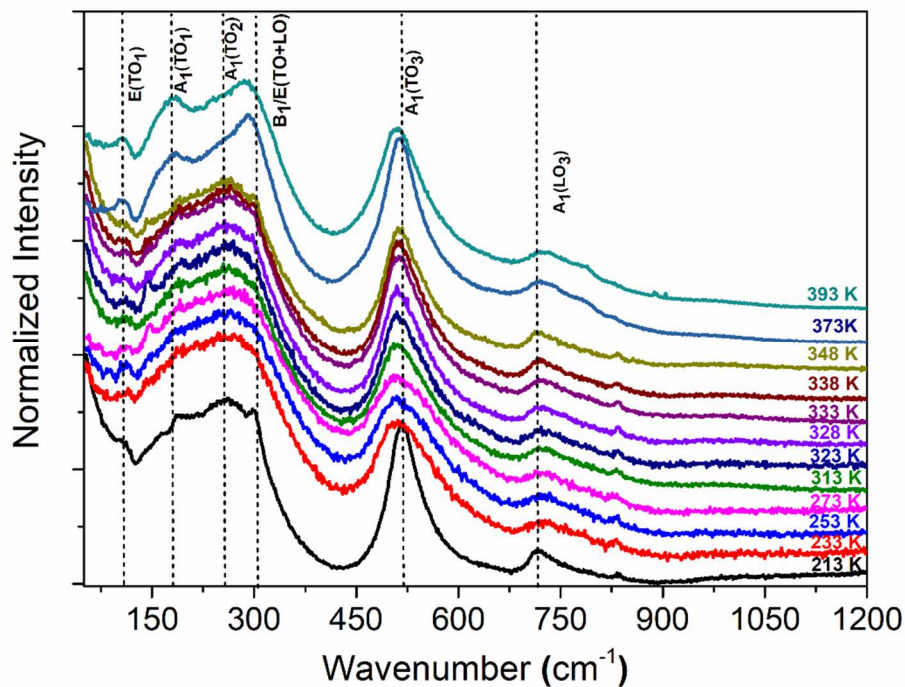


Fig. 8. Thermal variation of Raman spectra of the composition B₁EuZ₁T₁S

Noting that the measure was recorded within the temperature range 213 to 393K zone of the phase transition evidence by dielectric investigation. As can be seen from the figure, the peaks become broad with the increase of the temperature that is signature of a structural disorder resulting in the overlap of different Raman especially at a low wavenumber region that make very difficult to follow the thermal evolution of these modes, generally reported very sensitive to the phase transition in perovskite. Nevertheless, some changes could be spotted for A₁(TO₃) and A₁(LO₃) where they show a blue shift with increasing temperature.

The thermal variation of the peak position for both modes are given in the figure 9(a) and (b). As it can be deduced from the plots, clear anomalies are observed in the zone of the phase transition that corroborate the existence of the phase transition evidence by dielectric measurements

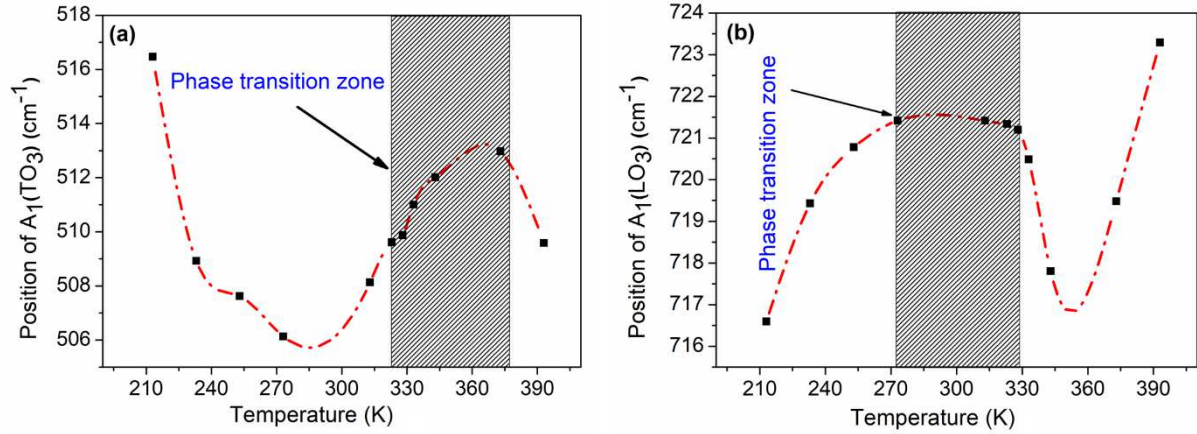


Fig.9. Variation of the peak position versus temperature of (a) $A_1(TO_3)$ mode ; (b) $A_1(LO_3)$ mode. The plots show anomalies in the T_c zone. lines are just guides for the eyes.

3.4. Photoluminescence study

Trivalent Europium (Eu^{3+} ; $4f^6$) is well known for its strong luminescence in the red spectral region. Many europium (III) compounds show an intense photoluminescence, due to the ${}^5D_0 \rightarrow {}^7F_j$ transitions ($J=0-6$) from the 5D_0 excited state to the J levels of the ground term 7F_j . The transition ${}^5D_0 \rightarrow {}^7F_0$ is strictly forbidden according to the standard Judd–Ofelt theory [49]. The occurrence of this transition is a well-known example of the breakdown of the selection rules of the Judd–Ofelt theory (a 0–0 transition is forbidden by the J selection rule of the Judd–Ofelt theory) [49]. Furthermore, the europium is habitually used as an optical sound to get supplementary structural information not accessible generally by structural refinement.

Fig.10 (a) shows the emission spectrum in the range 550-715 nm for the BEuZ5TS using an excitation length of 395 nm at room temperature. The PL spectrum presents 5 distinct bands characteristic of the emission of europium from the excited level 5D_0 to lower levels 7F_j ($j = 0,1,2,3,4$). The magnetic dipolar ${}^5D_0 \rightarrow {}^7F_1$ and the electric dipolar ${}^5D_0 \rightarrow {}^7F_2$ transitions are located around 596 nm and 611 nm respectively. Noting that the ${}^5D_0 \rightarrow {}^7F_3$ band is quite faint. This transition is generally forbidden according to the Judd–Ofelt theory, and this transition can only gain intensity via J -mixing [50]. A similar spectrum, with the same wavelength excitation, is observed for Eu^{3+} doped $BaZr_xTi_{1-x}O_3$ [51].

It should be noted that the transition ${}^5D_0 \rightarrow {}^7F_0$ is promising for technological applications because it reveals non-equivalent sites in a given host matrix [52]. In the present work, two excitation wavelengths have been used giving rise to a change in the PL spectrum. As it can be depicted in Fig.10 (b), the peak observed at 557 nm for an excitation wavelength of 390 nm appeared at 560 nm when the excitation is slightly changed to 395 nm, indicating the presence of at least two nonequivalent Eu^{3+} centers. Furthermore, the shoulder observed at ca. 580 nm disappeared and a new intense peak is developed at 587 nm, in addition to the appearance of a plateau-like between 600 and 630 nm. All these changes corroborate the existence of Eu^{3+} in two different environments. This assumption is in good agreement with the structural investigation reported above, where we suggested the possibility of the Eu_2O_3 presence as an impurity. For the compound with a high concentration of Zr (BEuZ20TS), the spectrum became dominated by a sharp ${}^5D_0 \rightarrow {}^7F_1$ transition as shown in Fig.10 (c). Indeed, the intensity of the ${}^5D_0 \rightarrow {}^7F_2$ and ${}^5D_0 \rightarrow {}^7F_4$ bands broaden and their intensities almost vanished. Our interest was also devoted to the trivalent holmium (Ho^{3+} ; $4f^{10}$) because it is considered as an important activator or sensitizer in near-infrared (NIR) region solid-state lasers [52, 54]. It has been also widely used in the visible region such as green and red emissions for many applications [55, 56]. It should be noted that Ho^{3+} based compounds exhibit an intense photoluminescence, due to the ${}^5F_0 \rightarrow {}^5I_J$ transitions ($J=0-8$) from the 5F_0 excited state to the J levels of the ground term $8I$ [57, 58]. Fig.10 (d) shows the emission spectrum in the range 500-800 nm for the two Ho-based compounds using an excitation length of 455 nm at room temperature. Noting that the BHoZ5TS spectrum exhibits two medium sharp peaks related to the green emission at 538 nm and 548 nm and one relatively weak band corresponding to the red emission at 681 nm. Further, one relatively weak band resulting to NIR emission situates at 754 nm. The green emission lines (at 540 and 548 nm) were assigned to the transition from the thermalized 5F_4 and 5S_2 states to the 5I_8 ground state. However, the red emission band is originating from the ${}^5F_5 \rightarrow {}^5I_8$ transition. While the NIR emission appearing at about 754 nm corresponds to the ${}^5F_5 \rightarrow {}^5I_7$ transition. Concerning BHoZ20TS composition, the profile of the PL spectrum is quite as that of BHoZ5TS and a wide low-intensity band between 640 and 660 nm is developed. Further, a NIR emission appearing at 742 nm and 753 nm could be attributed to the $({}^5F_5, {}^5S_2) \rightarrow {}^5I_7$ transitions.

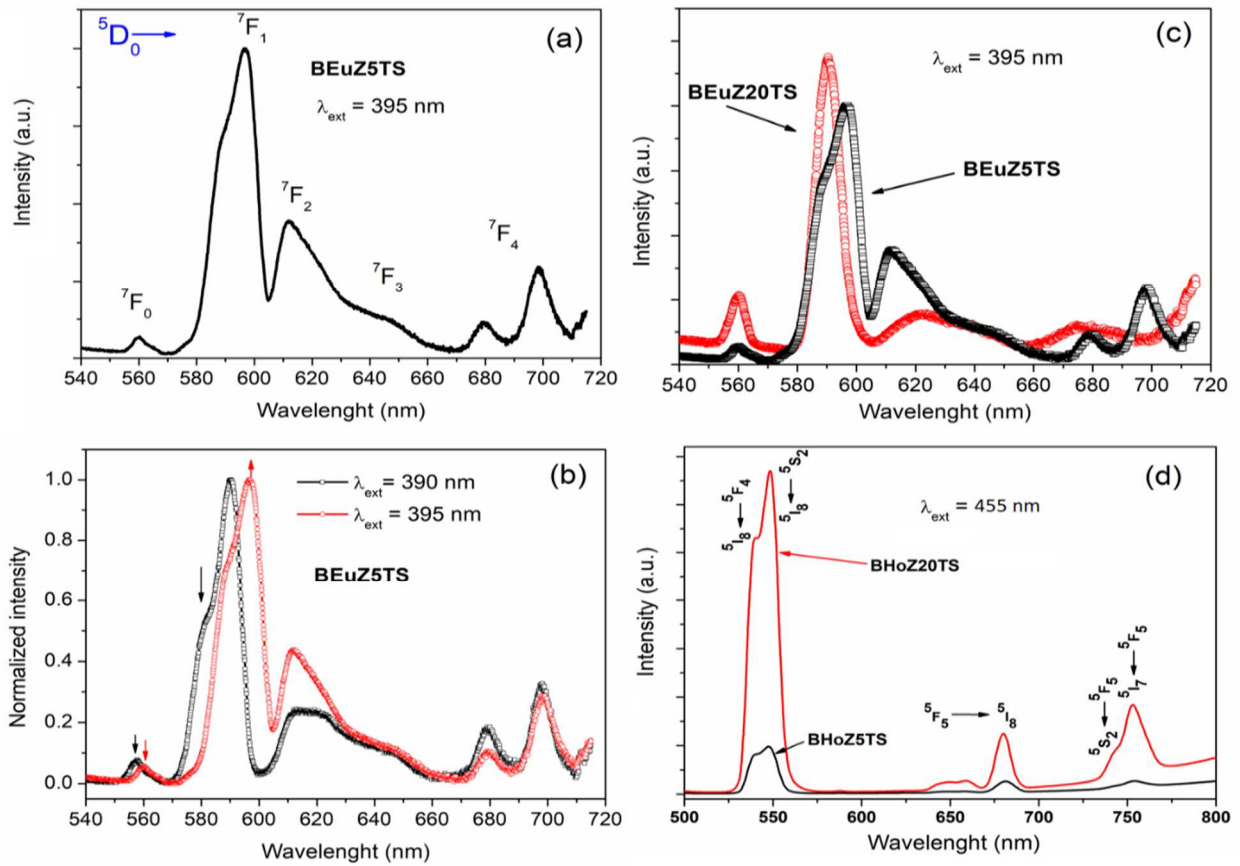


Fig.10: (a) PL emission spectrum of **BEuZ5TS** at an excitation wavelength of 395 nm at room temperature; (b) Normalized PL emission spectrum of **BEuZ5TS** at an excitation wavelength of 390 and 395 nm; (c) comparison of PL spectrum of **BEuZ5TS** and **BEuZ20TS** excited at 395 nm; (d) comparison of PL spectrum of **BHoZ5TS** and **BHoZ20TS** excited at 455 nm.

4. Conclusions

Lead-free $\text{Ba}_{0.975}\text{Ln}_{0.017}(\text{Ti}_{0.9}\text{Zr}_{0.05}\text{Sn}_{0.05})\text{O}_3$ (**BLnZ5TS**) and $\text{Ba}_{0.975}\text{Ln}_{0.017}(\text{Ti}_{0.75}\text{Zr}_{0.20}\text{Sn}_{0.05})\text{O}_3$ (**BLnZ20TS**) [$\text{Ln} = \text{Eu}, \text{Ho}$] ceramics, were successfully elaborated by conventional solid-state reaction. The SEM investigations showed a very marked modification in the grain size upon Ln^{3+} incorporation. Moreover, rare earth doping can promote grain growth and increase the density and uniformity of BZT ceramics. XRD spectra show that **BLnZ5TS** and **BLnZ20TS** ceramics still exhibit perovskite structure. Rietveld structural refinement of XRD data at room temperature endorsed respectively tetragonal and cubic symmetries for **BLnZ5TS** and **BLnZ20TS** compositions. The thermal and frequency variations of the permittivity revealed two kinds of behavior. Firstly, the normal ferroelectric with diffuse phase transition appearing for the low Zr content (**BLnZ5TS**) and the second is characteristic of relaxor ferroelectric for the higher Zr content composition (**BLnZ20TS**). T_m shifts towards

lower temperature when Zr content increases. For a fixed Zr content, T_m increases when the rare-earth radius decreases. The values ($T_0 > T_m$) observed for all compositions indicated the deviation from the Curie-Weiss law. The modified Curie Weiss law parameters confirmed the diffuse phase transition for all the compositions BLnZ5TS and BLnZ20TS. The close agreement of the data with the Vogel–Fülcher relationship suggests a relaxor like behavior for BLnZ20TS compositions. On the other hand, the photoluminescence study was performed considering Eu^{3+} as a structural probe. Two excitation wavelengths were used, giving slightly different response that tends to indicate the presence of two different sites of lanthanide. Further, Ho^{3+} is also used as a luminescent probe. Our optical study revealed that the higher zirconium content presents the higher signal compared to other zirconium contents. These results suggest that BLnZ20TS (Ln=Eu, Ho) could be a potential material for green and red emissions.

Acknowledgements

The authors gratefully acknowledge the financial support of the “Program Hubert Curien” (PHC-Tassili No. 18MDU107/39978VH); the Haute France Region/FEDER (project MASENE), and the European Union's Horizon 2020 research and innovation program ENGIMA.

References

- [1] Directive 2011/65/EU of the European Parliament and of the Council of 8 June 2011 on the Restriction of the Use of Certain Hazardous Substances in Electrical and Electronic Equipment Text with EEA Relevance (2011), <http://data.europa.eu/eli/dir/2011/65/oj/eng>.
- [2] T. Maiti, R. Guo, A.S. Bhalla, Electric field dependent dielectric properties and high tunability of $\text{BaZr}_x\text{Ti}_{1-x}\text{O}_3$ relaxor ferroelectrics, *Appl. Phys. Lett.* 89 (2006) 122909, <https://doi.org/10.1063/1.2354438.20>
- [3] Z. Yu, C. Ang, R. Guo, A.S. Bhalla, Dielectric properties and high tunability of $\text{Ba}(\text{Ti}_{0.7}\text{Zr}_{0.3})\text{O}_3$ ceramics under dc electric field, *Appl. Phys. Lett.* 81 (2002) 1285–1287, <https://doi.org/10.1063/1.1498496>.
- [4] U. Weber, G. Greuel, U. Boettger, S. Weber, D. Hennings, R. Waser, Dielectric properties of $\text{Ba}(\text{Zr}, \text{Ti})\text{O}_3$ -based ferroelectrics for capacitor applications, *J. Am. Ceram. Soc.* 84 (2001) 759–766, <https://doi.org/10.1111/j.1151-2916.2001.tb00738.x>.
- [5] X.G. Tang, K.-H. Chew, H.L.W. Chan, Diffuse phase transition and dielectric tunability of $\text{Ba}(\text{Zr}_y\text{Ti}_{1-y})\text{O}_3$ relaxor ferroelectric ceramics, *Acta Mater.* 52 (2004) 5177–5183,

<https://doi.org/10.1016/j.actamat.2004.07.028>

[6] Bell AJ, Deubzer O. Lead-free piezoelectrics-The environment and regulating issues. *MRS Bulletin*. 2018; 43 (8): 581-587. <https://doi.org/10.1557/mrs.2018.154>

[7] Acosta M. et al. BaTiO₃-based piezoelectrics: Fundamentals, current status and perspectives. *Applied Physics Reviews*. 2017; 4 (4): 041305. <https://doi.org/10.1063/1.4990046>.

[8] W. Xiaoyong, F. Yujun, Y. Xi, Dielectric relaxation behavior in barium stannate titanate ferroelectric ceramics with diffused phase transition, *Appl. Phys. Lett.* 83 (2003) 2031–2033, <https://doi.org/10.1063/1.1609037>.

[9] N. Horchidan, A.C. Ianculescu, L.P. Curecheriu, F. Tudorache, V. Musteata, S. Stoleriu, N. Dragan, D. Crisan, S. Tascu, L. Mitoseriu, Preparation and characterization of barium titanate stannate solid solutions, *J. Alloys Compd.* 509 (2011) 4731–4737, <https://doi.org/10.1016/j.jallcom.2011.01.123>.

[10] N. Haddadou, J. Belhadi, B. Manoun, K. Taïbi, B. Carcan, M. El Marssi, A. Lahmar, Structural, vibrational, and dielectric investigations of Ba_{0.925}Bi_{0.05}(Ti_{0.95-x}Zr_x)Sn_{0.05}O₃ ceramics, *J. Mater. Sci. Mater. Electron.* 29 (2018) 16144–16154, <https://doi.org/10.1007/s10854-018-9703-y>.

[11] C. Ostos, M.L. Martinez-Sarrion, L. Mestres, A. Cortes, E. Delgado, P. Prieto, Synthesis of new BLnZT nanostructured ferroelectric thin films, *Braz. J. Phys.* 36 (3B) (2006) 1062–1065, <https://doi:10.1590/S0103-97332006000600070>

[12] Y. Wang, L. Li, J. Qi, Z. Gui, Ferroelectric characteristics of ytterbium-doped barium zirconium titanate ceramics, *Ceram. Int.* 28 (2002) 657–661, [https://doi.org/10.1016/S0272-8842\(02\)00023-8](https://doi.org/10.1016/S0272-8842(02)00023-8).

[13] S.K. Ghosh, S.K. Rout, Induced instability in local structure and ferroelectric polarization of rare earth modified BZT relaxor ceramics, *Curr. Appl. Phys.* 16 (2016) 989–1000, <https://doi.org/10.1016/j.cap.2016.05.018>.

[14] F. Moura, A.Z. Simões, L.S. Cavalcante, M. Zampieri, J.A. Varela, E. Longo, M.A. Zaghete, Strain and vacancy cluster behavior of vanadium and tungsten-doped Ba[Zr_{0.10}Ti_{0.90}]O₃ ceramics, *Appl. Phys. Lett.* 92 (2008) (032905-1- 032905-3), <https://doi.org/10.1063/1.2837196>.

[15] H. Feng, J. Hou, Y. Qu, D. Shan, G. Yao, Structure, dielectric and electrical properties of cerium doped barium zirconium titanate ceramics, *J. Alloy. Compd.* 512 (1) (2012) 12–16, <https://doi.org/10.1016/j.jallcom.2011.08.015>.

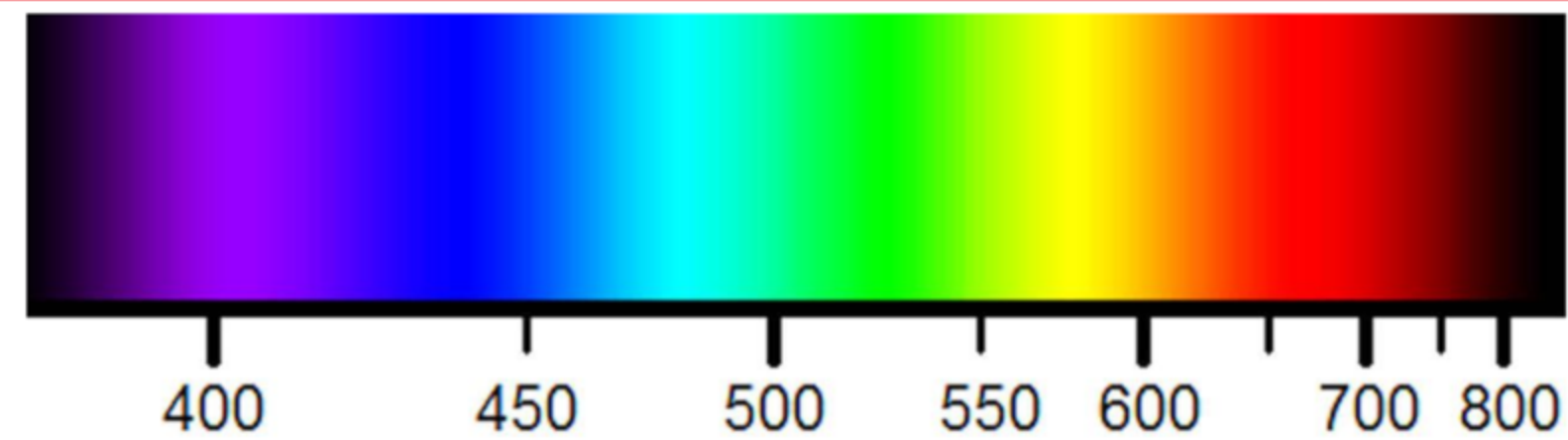
- [16] C. Ostos, L. Mestres, M.L. Martinez-Sarrio, J.E. Garcia, A. Albareda, R. Perez, Synthesis and characterization of A-site deficient rare-earth doped $\text{BaZr}_x\text{Ti}_{1-x}\text{O}_3$ perovskite-type compounds, *Solid State Sci.* 11 (2009) 1016–1022, <https://doi.org/10.1016/j.solidstatesciences.2009.01.006>.
- [17] S. Smail, M. Benyoussef, K. Taïbi, N. Bensemma, B. Manoun, M. El Marssi, A. Lahmar, Structural, dielectric, electrocaloric and energy storage properties of lead free $\text{Ba}_{0.975}\text{La}_{0.017}(\text{Zr}_x\text{Ti}_{0.95-x})\text{Sn}_{0.05}\text{O}_3$ ($x=0.05; 0.20$) ceramics, *Materials Chemistry and Physics* 252 (2020) 123462, <https://doi.org/10.1016/j.matchemphys.2020.123462>
- [18] X. Chou, J. Zhai, H. Jiang, X. Yao, Dielectric properties and relaxor behavior of rare-earth (La, Sm, Eu, Dy, Y) substituted barium zirconium titanate ceramics, *J. Appl. Phys.* 102 (2007) 084106, <https://doi.org/10.1063/1.2799081>
- [19] T. Badapanda, V. Senthil, S. Panigrahi, S. Anwar, Diffuse phase transition behavior of dysprosium doped barium titanate ceramic, *J. Electroceram.* 31 (1–2) (2013) 55–60, <https://doi.org/10.1007/s10832-013-9808-x>
- [20] Agda E. Souza, Guilherme S. Sasaki, Sabrina A. Camacho, Silvio R. Teixeira, Maximo S. Li, Elson Longo, Defects or charge transfer: Different possibilities to explain the photoluminescence in crystalline $\text{Ba}(\text{Zr}_x\text{Ti}_{1-x})\text{O}_3$ *J. Lumin.*, 179(2016)132–138. <https://doi.org/10.1016/j.jlumin.2016.06.033>
- [21] C. Ciomaga, M. Viviani, M.T. Buscaglia, V. Buscaglia, L. Mitoseriu, A. Stancu, Preparation and characterization of the $\text{Ba}(\text{Zr Ti})\text{O}_3$ ceramics with relaxor properties, *J. Eur. Ceram. Soc.* 27 (2007) 4061–4064. <https://doi.org/10.1016/j.jeurceramsoc.2007.02.095>
- [22] A. Boultif, D. Louer, Indexing of powder diffraction patterns for low-symmetry lattices by the successive dichotomy method, *J. Appl. Crystallogr.* 24 (1991) 987–993, <https://doi.org/10.1107/S0021889891006441>.
- [23] T. Roisnel, J. Rodriguez-Carvajal, WinPLOTR: a windows tool for powder diffraction pattern analysis, *Mater. Sci. Forum* 378–381 (2001) 118–123 <https://doi.org/10.4028/www.scientific.net/MSF.378-381.118>
- [24] G.H. Kwei, A.C. Lawson, S.J.L. Billinge, S.W. Cheong, Structures of the ferroelectric phases of barium titanate, *J. Phys. Chem.* 97 10(1993)2368–2377. <https://doi.org/10.1021/j100112a043>
- [25] S. Bhaskar Reddy, K. Prasad Rao, M.S. Ramachandra Rao, Effect of La substitution on the structural and dielectric properties of $\text{BaZr}_{0.1}\text{Ti}_{0.9}\text{O}_3$ ceramics, *J. Alloys Compd.* 481 (2009) 692–696, <https://doi.org/10.1016/j.jallcom.2009.03.075>.

- [26] R. Kumar, K. Asokan, S. Patnaik, B. Birajdar, Combined effect of oxygen annealing and La-doping in broadening the phase transition of Ba(Zr_{0.2}Ti_{0.8})O₃ ceramics, *J. Alloys Compd.* 737 (2018) 561–567, <https://doi.org/10.1016/j.jallcom.2017.11.344>.
- [27] R. Kumar, K. Asokan, S. Patnaik, Birajdar, Evolution of relaxor ferroelectric properties in La-doped barium zirconate titanate, *Ferroelectrics* 517 (2017) 8-13, <https://doi: 10.1080/00150193.2017.1369820>
- [28] M. Benyoussef, M. Zannen, J. Belhadi, B. Manoun, J.-L. Dellis, M. El Marssi, A. Lahmar, Dielectric, ferroelectric, and energy storage properties in dysprosium doped sodium bismuth titanate ceramics, *Ceram. Int.* 44 (2018) 19451–19460 <https://doi.org/10.1016/j.ceramint.2018.07.182>
- [29] R.D. Shannon Revised effective ionic radii and systematic studies of interatomic distances in halides and chalcogenide. *Acta Crystallogr.* A32 (1976) 751–767. <https://doi.org/10.1107/S0567739476001551>
- [30] Y.Tsur, T.D. Dunbar and C.A. Randall, crystal and defect chemistry of rare earth cations in BaTiO₃, *J. Electroceram.*, 7, (2001) 25–34. <https://doi.org/10.1023/A:1012218826733>
- [31] L.E. Cross, Relaxor ferroelectrics: an overview, *Ferroelectrics* 151 (1994) 305–320, <https://doi.org/10.1080/00150199408244755>.
- [32] K. Uchino, Relaxor ferroelectric devices, *Ferroelectrics* 151 (1994) 321–330, <https://doi.org/10.1080/00150199408244756>.
- [33] X. Diez-Betriu, J.E. Garcia, C. Ostos, A.U. Boya, D.A. Ochoa, L. Mestres, R. Perez, Phase transition characteristics and dielectric properties of rare-earth (La, Pr, Nd, Gd) doped Ba(Zr_{0.09}Ti_{0.91})O₃ ceramics, *Mater. Chem. Phys.* 125 (2011) 493–499, <https://doi:10.1016/j.matchemphys.2010.10.027>.
- [34] S.B. Reddy, K.P. Rao, M.S. Ramachandra Rao, Influence of A-site Gd doping on the microstructure and dielectric properties of Ba(Zr_{0.1}Ti_{0.9})O₃ ceramics, *J. Alloy. Compd.* 509 (2011) 1266–1270. <https://doi.org/10.1016/j.jallcom.2010.09.211>
- [35] W. Cai, C. Fu, J. Gao, Z. Lin, X. Deng, Effect of hafnium on the microstructure, dielectric and ferroelectric properties of Ba[Zr_{0.2}Ti_{0.8}]O₃ ceramics, *Ceram. Int.* 38 (2012) 3367–3375. <https://doi10.1016/j.ceramint.2011.12.047>
- [36] T. Badapanda, S. Sarangi, B. Behera, S. Anwar, T.P. Sinha, R. Ranjan, G.E. Luz, E. Longo, L.S. Cavalcante, Structural refinement, optical and electrical properties of Ba_{1-x}Sm_{2x/3}(Zr_{0.05}Ti_{0.95})O₃ ceramics, *J. Mater. Sci. Mater. Electron.* 25 (2014) 3427–3439, <https://doi.org/10.1007/s10854-014-2035-7>

- [37] Chen Zhang · Fangxu Chen · Xin Zhong · Zhixin Ling · Zhuming Tang · Gang Jian, Enhanced ferroelectric relaxor behavior of Ho₂O₃-modified barium zirconate titanate ceramics, *J. Mater. Sci. Mater. Electron.*, 29 (2018) 16730–16739
<https://doi.org/10.1007/s10854-018-9766-9>
- [38] G. Nag Bhargavi, A. Khare, T. Badapanda, P. K. Ray, N. Brahme, Influence of Eu doping on the structural, electrical and optical behavior of Barium Zirconium Titanate ceramic, *Ceramics International* 44 (2018) 1817–1825,
<https://dx.doi.org/10.1016/j.ceramint.2017.10.116>
- [39] G.N. Bhargavi, A. Khare, T. Badapanda, M.S. Anwar, Investigation of structural and electrical properties of Gd³⁺ ions modified BaZr_{0.05}Ti_{0.95}O₃ ceramic, *Appl. Phys. A124*, 11 (2018) 1-9. <https://doi.org/10.1007/s00339-018-2162-8>
- [40] M. Benyoussef, M. Zannen, J. Belhadi, B. Manoun, J.-L. Dellis, A. Lahmar, M. El Marssi, Complex impedance and Raman spectroscopy of Na_{0.5}(Bi_{1-x}Dy_x)_{0.5}TiO₃ ceramics, *Ceram. Int.*46 (2020) 10979–10991 <https://doi.org/10.1016/j.ceramint.2020.01.114>.
- [41] W. Kang, Z. Zheng, Y. Li, R. Zhao, W. Dun, Y. Wang, Effect of doping Gd₂O₃ on dielectric and piezoelectric properties of BaZr_{0.1}Ti_{0.9}O₃ ceramics by sol–gel method, *J. Mater. Sci. Mater. Electron.*30 (2019) 2743–2749,
<https://doi.org/10.1007/s10854-018-0550-7>
- [42] M. Ravez, P. Pouchard, P. Hagenmuller, Chemical bonding and ferroelectric perovskite, *Eur. J. Solid State Inorg. Chem*, vol.28 (1991)1107.
- [43] X. G. Tang, X. X. Wang, K-H Chew, H.L.W Chan, Relaxor behavior of (Ba,Sr)(Zr,Ti)O₃ ferroelectric ceramics. *Solid State Communications*, 136 (2) (2005) 89-93
<https://doi.org/10.1016/j.ssc.2005.06.034>
- [44] G.A. Smolenskii, Physical phenomena in ferroelectrics with diffused phase transition, *J. Phys. Soc. Japan*, 28 Suppl. (1970) 26-37
- [45] K. Uchino and S. Nomura, Critical exponents of the dielectric constant in diffused-phase transition crystals, *Ferroelectrics Lett.* 44 (1982) 55-61,
<https://doi.org/10.1080/00150198208260644>
- [46] D.Viehlang, S.J. Jang and L.E. Cross, Freezing of the polarization fluctuations in lead magnesium niobate relaxors, *J. Appl. Phys.*, 68(6) (1990) 2916-2921.
<https://doi.org/10.1063/1.346425>
- [47] L.E. Cross, Relaxor ferroelectrics, *Ferroelectrics*, 76 (1987) 241-267.
<https://doi.org/10.1080/00150198708016945>

- [48] C. Lauhlé, F. Hippert, R. Bellissent, A. Simon, and G. J. Cuello, Local structure in BaTi_{1-x}Zr_xO₃ relaxors from neutron pair distribution function analysis, *Phys. Rev. B* 79, (2009) 064104. <https://doi.org/10.1103/PhysRevB.79.064104>
- [49] K. Binnemans, Interpretation of europium (III) spectra, *Coord. Chem. Rev.*, 295 (2015) 1–45. <https://doi.org/10.1016/j.ccr.2015.02.015>
- [50] J.E. Lowther, Spectroscopic transition probabilities of rare earth ions, *J. Phys. C: Solid State Phys.*, 7 (1974) 4393–4402. <https://doi.org/10.1088/0022-3719/7/23/026>
- [51] G. Canu, G. Bottaro, M. T. Buscaglia, C. Costa, O. Condurache, L. Curecheriu, L. Mitoseriu, V. Buscaglia and L. Armelao, Ferroelectric order driven Eu³⁺ photoluminescence, in BaZr_xTi_{1-x}O₃ perovskite, *Sci. Rep.*, 9 (2019) 6441-6452. <https://doi.org/10.1038/s41598-019-42897-1>
- [52] H. Gobrecht, Über die Absorptions- und Fluoreszenzspektren der Ionen der Seltenen Erden in festen Körpern, insbesondere im Ultrarot, *Ann. Der Phys.*, 28 (1937) 673–700. <https://doi.org/10.1002/andp.19374200802>
- [53] L.F. Johnson, H.J. Guggenheim, T.C. Rich, F.W. Ostermayer, Infrared-to-Visible Conversion by Rare-Earth Ions in Crystals, *J. Appl. Phys.*, 43 (1972) 1125. <https://doi.org/10.1063/1.1661225>
- [54] B.M. Antipenko, B.V. Vorykhalov Sinitsyn, T.V. Uvarova, Laser frequency converter based on a BaYb₂F₈:Ho³⁺ crystal. Stimulated emission at 2μ, *Sov. J. Quantum Electron.* , 10 (1980) 114. <https://doi.org/10.1070/QE1980v010n01ABEH009873>
- [55] H.J. Guggenheim and L.F. Johnson, New fluoride compounds for efficient infrared to visible conversion, *Appl. Phys. Lett.* , 15 (1969) 51. <https://doi.org/10.1063/1.1652898>
- [56] K. Yang, S. Zhao, G. Li, Diode-pumped Actively Q-switched Nd: GdVO₄ Green Laser with Periodically Poled KTP, *Opt. Quantum Electron.*, 37 (2005) 875-887. <https://doi.org/10.1007/s11082-005-8121-6>
- [57] T. Zhang, J. Wang, J. Jiang, R. Pan, B. Zhang, Microstructure and photoluminescence properties of Ho-doped (Ba,Sr)TiO₃ thin films, *Thin Solid Films*, 515 (2007) 7721–7725. <https://doi.org/10.1016/j.tsf.2007.03.010>
- [58] J. Wang, T. Zhang, R. Pan, Z. Maa, J. Wang, Spectroscopic and photoluminescence properties of Ho³⁺ doped Ba_{0.65}Sr_{0.35}TiO₃ nanocrystals, *Physica B*, 407 (2012) 160–164. <https://doi.org/10.1016/j.physb.2011.10.009>

$\lambda_{\text{ext}} = 395 \text{ nm}$



BEuZ20TS

BEuZ5TS

